論文 / 著書情報
Article / Book Information

Title	Numerical simulations of all-solid-state batteries using specific contact area diameters for active materials determined by X-ray computed tomography
Authors	S. Iwamoto, M. Kodama, K. Yanagi, Y. Haniu, Y. Fujii, N. Masuda, H. Higuchi, Y. Suetsugu, S. Hirai
Citation	Journal of Power Sources Advances, Volume 21, , 100120
Pub. date	2023, 6
DOI	https://dx.doi.org/10.1016/j.powera.2023.100120

Journal of Power Sources Advances 21 (2023) 100120

Contents lists available at ScienceDirect

Journal of Power Sources Advances

journal homepage: www.sciencedirect.com/journal/journal-of-power-sources-advances

Numerical simulations of all-solid-state batteries using specific contact area diameters for active materials determined by X-ray computed tomography

S. Iwamoto [a], M. Kodama [a,*], K. Yanagi [b], Y. Haniu [b], Y. Fujii [b], N. Masuda [b], H. Higuchi [b], Y. Suetsugu [b], S. Hirai [a]

[a] Tokyo Institute of Technology, 2-12-1 Ookayama, Meguro-ku, Tokyo, 152-8550, Japan
[b] Idemitsu Kosan Co., Ltd., 1280 Kami-izumi, Sodegaura-shi, Chiba, 299-0293, Japan

ARTICLE INFO

Keywords:
All-solid-state lithium-ion battery
P2D simulation
X-ray CT
Specific contact area diameter

ABSTRACT

At present, it would be desirable to improve the C-rate values of bulk-type all-solid-state lithium-ion batteries by optimizing the electrode structures. Although simulations are an effective means of determining optimal structures, a high degree of accuracy is required. The present study demonstrates a pseudo-two-dimensional (P2D) method of simulating cathodes providing improved accuracy along with low computational cost and based on actual three-dimensional electrode structures. This method incorporates the volume fraction and tortuosity of the solid electrolyte (SE) and active material (AM), both of which are widely used in conventional simulations, and takes into account the specific contact area diameter (D_{SCA}) of the AM. The latter parameter reflects the extent of AM particle aggregation and is obtained from the analysis of three-dimensional X-ray computed tomography images. The validity of these P2D simulations is confirmed by comparison with experimental results for three electrodes having different SE particle sizes. The experimental result shows that battery capacity is increased with decreases in the SE particle sizes. This effect is not predicted using conventional P2D simulations employing only volume fraction and tortuosity but is reproduced by P2D simulations in which D_{SCA} values are used to model AM particle aggregation and Li diffusion within AM particles.

1. Introduction

The shift from gasoline-powered vehicles to electric vehicles (EVs) has resulted in a drive to develop next-generation EVs, with much of this research focused on long-range cruising and fast charging/discharging. A key component of any EV is its rechargeable battery and batteries exhibiting high capacity, high power input and high power output are required for next-generation EVs [1]. Conventional EVs use lithium-ion batteries (LiBs) based on liquid organic compounds acting as electrolytes. Unfortunately, these compounds are flammable and so have associated safety concerns [2]. In contrast, all-solid-state LiBs (ASSLiBs) with sulfide solid electrolytes (SEs) are expected to exhibit fast charging/discharging with a low risk of combustion [3]. The electrodes in the bulk-type ASSLiBs that are likely to be employed as high-capacity batteries in newer EVs contain both an active material (AM) and an SE. Rapid ion transportation within the SE network, suitably fast interfacial reactions at the SE-AM interface and smooth lithium diffusion within AM particles will all be required to produce high-performance bulk-type ASSLiBs and could be satisfied by optimization of the electrode structure.

Many experimental studies have examined the relationship between electrode structure and the performance of bulk-type ASSLiBs [4–6]. As an example, Siroma et al. used AC impedance measurements to determine that the ionic conductivity of the electrode can be changed by varying the AM volume ratio. It has also been reported that the facile transportation of electrons and lithium ions is a necessary prerequisite for high battery capacity [4]. In addition, Strauss et al. demonstrated that the electronic conductivity associated with atomization of the AM contributes to achieving high capacity in such batteries [5]. Otoyama et al. assessed the state of charge distribution in the AM after charging using Raman spectroscopy. Their work established that this parameter was lowered by aggregation of the AM as a consequence of a reduced AM-SE contact area together with increases in the lithium diffusion length in the AM [6].

These previous studies suggest that the electrode should be constructed to promote the transport of lithium ions and electrons while

* Corresponding author.
E-mail address: tanaka.m.ay@m.titech.ac.jp (M. Kodama).

https://doi.org/10.1016/j.powera.2023.100120
Received 25 March 2023; Received in revised form 26 May 2023; Accepted 30 May 2023
Available online 2 June 2023

also enhancing interfacial reactions and diffusion in the AM so as to achieve high-performance ASSLiBs. However, because various factors can affect the electrode structure (such as the mixing method, volume fraction and particle size of the AM and SE), the efficient optimization of these batteries via experimentation is very difficult. For this reason, numerical simulations involving low computational costs are a useful alternative approach to the structural optimization of electrodes. In particular, pseudo-two-dimensional (P2D) simulations performed in bulk-type ASSLiBs can provide lower computational costs compared with three-dimensional (3D) simulations [7].

The Newman model is one means of performing numerical simulations of batteries and has been previously applied in this manner [8–10]. One possible factor related to electrode structure that can affect electrode performance is the lithium-ion migration distance in the SE. This distance is reflected by a variable referred to as tortuosity. In prior work, Wolff et al. considered the effect of electrode structure on ionic conductivity using tortuosity values calculated using Bruggeman's equation [10,11]. However, the tortuosity obtained in this manner has been reported to be lower than that calculated from experimental data and so this type of analysis cannot accurately assess the effects of electrode structure [12]. Just as P2D simulation of LiBs has improved accuracy by reflecting 3D structures [13], P2D simulation of ASSLiBs has also been studied to improve accuracy by using 3D structures. Hlushkou et al. conducted simulations using the tortuosity values calculated from 3D electrode structures obtained from focused ion beam scanning electron microscopy images [14]. In addition, Kashkooli et al. obtained tortuosity data using 3D electrode structures generated using X-ray computed tomography (CT). The resulting simulations reproduced the C-rate characteristics of the device with improved accuracy compared with calculations using tortuosity values obtained from Bruggeman's equation [15].

Simulations employing a 3D electrode structure can allow the effects of the structure to be more accurately reflected in the calculations. However, these effects are not solely associated with tortuosity and volume fraction, as has been assumed in previous simulations of ASSLiBs [15]. The contact area between the AM and SE together with the lithium diffusion distances in the AM particles will also determine battery performance, because these factors can induce an overpotential as a result of reaction resistance and diffusion resistance. The contact area and lithium diffusion distance are, in turn, related to the extent of aggregation of the AM particles, and the effect of this aggregation will be more significant in ASSLiBs than in liquid LiBs. This difference can be attributed to the small gaps between aggregated AM particles in liquid LiBs, through which the liquid electrolyte can migrate to produce ion transportation paths. In contrast, the SE particles in ASSLiBs cannot penetrate into the aggregated AM particles. Therefore, the effect of AM particle aggregation should be incorporated into simulations of ASSLiBs to ensure a high degree of accuracy.

Several previous simulations of liquid LiBs have considered the effects of AM particle aggregation [16–18]. Wang et al. conducted discharge simulations of liquid LiB electrodes composed of AMs having different particle diameters and found that the discharge capacity increased with decreases in the AM particle size because of an associated decrease in the diffusion distance [16]. Awaker et al. conducted an electrolytic analysis of liquid LiB electrodes composed of AMs with varying particle sizes and found that the frequency of contact between the conductive agent and the AM increased with increases in particle size and that this, in turn, improved conductivity [17]. Goldin et al. reproduced the decrease in discharge capacity resulting from a loss of contact area between the AM and the electrolyte caused by aggregation of the AM by calculating an effective particle radius associated with the specific contact area in a liquid LiB [18].

As described above, highly accurate P2D simulations of liquid LiBs must incorporate the effects of AM particle aggregation in addition to the more commonly used parameters of volume fraction (ε) and tortuosity (τ). In the case of simulations involving ASSLiBs, it is even more important to consider the effects of AM particle aggregation based on determining the specific contact area between the AM and the SE, such as via the effective particle radius value previously used to model liquid LiBs [18].

Although the importance of reflecting 3D structure in P2D simulations has been demonstrated, the case of reflecting active material aggregation based on 3D structure in P2D simulations has hardly been confirmed for P2D simulation of ASSLiB. Therefore, in the present study, a new approach was developed for P2D simulation of ASSLiB using X-ray CT to determine the AM-specific contact area diameter (D_{SCA}) as an indicator of the extent of aggregation. The validity of these simulations was verified by comparison with experimental results for three electrodes having different SE particle sizes.

2. Experimental and numerical procedures

The accuracy of the present P2D simulations based on D_{SCA} values was assessed by performing discharge experiments and P2D discharge simulations using structural parameters obtained from X-ray CT. The simulation results were compared with the discharge experiment results.

2.1. Experimental procedures

2.1.1. Cathode half-cell discharge experiment procedures

The cathode composite was prepared by mechanically mixing $Li_4Ti_5O_{12}$-coated $LiNi_{0.8}Co_{0.15}Al_{0.05}O_2$ (NCA) and $75Li_2S–25P_2S_5$ glass (LPS) powders. The median diameter of the NCA was 5 μm while the median diameter of the LPS was 1, 2 or 6 μm. The electrical conductivities of the NCA and LPS were 910 and 0.45 mS/cm, respectively. These materials were combined at 85 and 15 wt%, respectively, then sealed in a zirconia pot along with 34 g of zirconia balls (2 mm diameter) and mechanically mixed at 600 rpm for 1 h using a rolling mill (AV-1, Asahi Rika Seisakujo). All the materials were processed in an argon-filled glove box with a low dew point (<-70 °C).

Following this, the cathode half-cell was assembled in the glove box. A 90 mg quantity of LPS was transferred into a cell consisting of a 10 mm diameter Macor cylinder and a stainless-steel current collector. After pressing this material at 185 MPa, 12.4 mg of the cathode composite was inserted into the same cell and the combined sample was pressed at 555 MPa. These procedures fabricated a cathode having a thickness of 43 μm into which a section of lithium metal was inserted as a counter electrode. Finally, the resulting cell was pressed at 93 MPa and then clamped at 30 MPa.

The cathode half-cell was sealed in a container and discharge tests were conducted outside the glove box. These trials were performed over the potential range of 4.2 − 3.1 V vs Li^+/Li and the constant current range of 0.189–15.12 mA (0.1 C − 4 C) using a battery testing system.

2.1.2. X-ray CT procedures

Samples of the compressed cathodes were cut out using a 0.3 mm diameter hand punch (NOGAMI) in preparation for X-ray CT analysis. The sample size was selected so as to ensure sufficient X-ray transmission to allow for high resolution. These samples were transferred into an airtight jig made of polyetheretherketone (PEEK) inside a nitrogen-filled glove box with a low dew point (<-70 °C). The jig also contained molecular sieves (type 3A, Kanto Chemical) to remove any water vapor adsorbed on the inner walls [19].

Each cathode sample was assessed using X-ray CT (Rigaku, customized nano3DX) with a voxel size of 325 × 325 × 325 nm. A rotating electrode-type X-ray generator was employed, operating at 45 kV and 66 mA with a molybdenum target [20]. The CT images were reconstructed from a series of X-ray transmission images. In these images, the AM (which had a high X-ray absorption coefficient) appeared white while the SE (with a low coefficient) appeared black, making it possible to identify the components of the cathode.

2.2. Numerical procedures

The numerical procedures below are based on 3D X-ray CT images. To obtain these images, a 3D box smoothing filter in MATLAB is used to reduce noise. The active material and solid electrolyte were identified by setting the X-ray CT image threshold to match their respective volume fractions in the electrode, determined from the weight ratio of the composite material.

2.2.1. Calculation of tortuosity and specific contact area diameter from X-ray CT images

The tortuosity values related to the electron and ion migration pathways in the AM and SE, respectively, were determined using an electric field analysis based on the X-ray CT 3D images [20–22]. As noted, the extent of AM particle aggregation can be quantitatively evaluated based on the specific contact area of the material ($S_{AM\text{-}SE}$). This can be defined using the specific contact area diameter (D_{SCA}) per unit volume and the number of AM aggregates per unit volume (N_{AM}) as

$$S_{AM-SE} = N_{AM} 4\pi \left(\frac{D_{SCA}}{2}\right)^2. \quad (1)$$

The corresponding volume of the AM (V_{AM}) can be calculated using the equation

$$V_{AM} = N_{AM} \frac{4}{3}\pi \left(\frac{D_{SCA}}{2}\right)^3. \quad (2)$$

From these two equations, we have

$$D_{SCA} = \frac{6V_{AM}}{S_{AM-SE}}. \quad (3)$$

The values of both V_{AM} and $S_{AM\text{-}SE}$ could be obtained from the X-ray CT images, allowing D_{SCA} to be calculated. In this case, $S_{AM\text{-}SE}$ calculated by taking into account the increase in SE-AM contact area due to voxelization in the X-ray CT images. Because this parameter reflects the AM agglomeration structure, it represents the effective particle diameter.

P2D simulations cannot accurately reproduce the complex shapes of real electrodes because the active material is treated as a spherical shape. In the presented method, the complex active material shape is converted to spherical shape by using the D_{SCA} such that the accuracy of the model is improved as much as possible.

2.2.2. Modeling and simulation

Discharge simulations were performed on a cathode half-cell based on the P2D ASSLiB model proposed by Wolff et al. [10]. Wolff's model can simulate the structural characteristics of the solid electrolyte. However, the active material diameters used in this model is only its non-aggregated case of the diameter cannot simulate the aggregation of the active material. Therefore, reflecting the aggregation of the active material in this model is expected to achieve more accurate simulation. So, in this numerical simulation, D_{SCA} explained above is used to the effective active material diameter. As in Wolff's model, the electrochemical reaction at the AM-SE interface, lithium-ion (Li^+) transport through the SE and electron (e^-) transport through the AM are simulated in a single dimension (x) corresponding to the thickness direction of the cell. In contrast, lithium (Li) diffusion through the AM is modeled in a pseudo-dimension (r) within the AM particles. The diffusion coefficient of Li in the AM depends on the Li concentration measured in the experiment [23]. The AM particle size included in these simulations was either the median particle diameter used in previous studies or the D_{SCA} value calculated from X-ray CT 3D images. In addition, the τ_{SE} and τ_{AM} values obtained from X-ray CT 3D images were used to determine the effective Li^+ conductivity and electron transport values.

3. Results and discussion

3.1. X-ray CT structural analyses

Fig. 1 (a)–(c) present X-ray CT images of SE specimens having varying particle sizes. Fig. 1 (d), (e) and (f) summarizes the tortuosity of the AM (τ_{AM}), the tortuosity of the SE (τ_{SE}) and the D_{SCA} for each SE particle size as calculated from X-ray CT images. The data in Fig. 1 (d) and (e) demonstrate that the tortuosity values of the AM and SE were independent of the LPS particle size. In contrast, the D_{SCA} increased along with the SE particle size, as demonstrated by Fig. 1 (f). It is likely that smaller SE particles were inserted between the AM particles such that the aggregation of the AM was inhibited, thus reducing the D_{SCA}.

3.2. Comparison of simulated and experimental battery performance data

Discharge experiments and simulations were conducted for cathodes having varying SE particle sizes. Fig. 2 (a) plots the discharge capacities as functions of the C-rates measured in the experiments. Fig. 2 (b) plots the discharge capacities as function of the C-rates calculated in the P2D simulations. These simulations were based on the volume fractions and tortuosity values (that is, τ_{AM} and τ_{SE}) obtained from X-ray CT 3D images and the AM median particle diameter ($D50_{AM}$ = 5 μm). Fig. 2 (d) plots the absolute differences between the experimental and simulated capacities obtained using the $D50_{AM}$ value (ΔCapacity). Fig. 2 (c) shows the discharge capacities plotted against the C-rates calculated from the P2D simulations, based on the volume fractions and the tortuosity values (τ_{AM}, τ_{SE}) generated using X-ray CT 3D images in conjunction with the AM-specific contact area diameter (D_{SCA}). Fig. 2 (e) presents the absolute differences between the experimental and simulated capacities obtained using the D_{SCA} (Δ Capacity). From Fig. 2 (a) it is evident that the experimental discharge capacity decreased with increases in the C-rate at all SE particle sizes and that the discharge capacity at 1 C was lower for the 6-μm particles compared with the 1- and 2-μm particles. As shown in Fig. 2 (b), the decrease in the discharge capacity with increases in the C-rate could be simulated using $D50_{AM}$ although the drop in discharge capacity associated with 6-μm SE particles was not accurately predicted. In contrast, simulations using the D_{SCA} value successfully reproduced the decreased discharge capacity obtained with 6-μm SE particles. The differences in capacity from the experimental data were generally smaller in the case of simulations performed with the D_{SCA} value (Fig. 2 (e)) than for those using $D50_{AM}$ (Fig. 2 (d)). Thus, the former simulations reproduced the experimental discharge capacity more accurately. It should also be noted that the simulations employing D_{SCA} exhibited the greatest differences from experimental values at 2 C with 1- and 2-μm SE particles, although these discrepancies were less than 10 mAh/g and so not significant in practical terms.

The experimental discharge curves are presented in Fig. 3 (a) while the P2D simulations with $D50_{AM}$ and with D_{SCA} for 2-μm SE particles are shown in Fig. 3 (b) and (c), respectively. It is apparent that both types of simulations correctly predicted the voltage drop at the start of the discharge (0 mAh/g). This outcome indicates that P2D simulations using both $D50_{AM}$ and D_{SCA} can provide correct values for the ion transportation resistance in the SE as well as the interface resistance between the SE and AM. Even so, the discharge capacity plots obtained from the simulations involving $D50_{AM}$ and D_{SCA} differ from one another, particularly in the last half of each plot. Specifically, the capacity values generated using the D_{SCA} method are much closer to the experimental data. The greater accuracy of this approach is attributed to improved modeling of Li diffusion in the AM particles.

In this study, aggregation and agglomeration are not distinguished, and they are treated together as aggregation in the simulation, but the simulation accuracy is higher than that of the conventional method using the median particle size as described above. It is believed that distinguishing between them can simulate Li diffusion more accurately and increase the simulation accuracy. Moreover, the improvements in

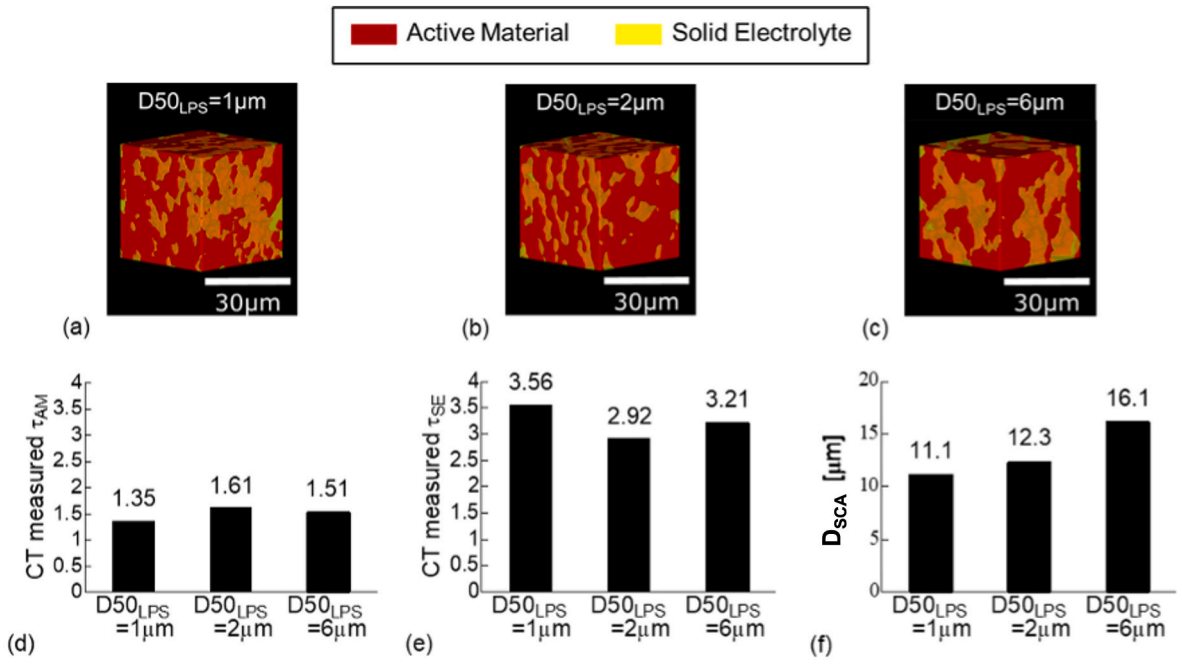

Fig. 1. X-ray CT images of electrodes with solid electrolytes having $D50_{LPS}$ of (a) 1, (b) 2 and (c) 6 μm. Legend: red = AM, yellow = SE. The values for various structural parameters for each $D50_{LPS}$: (d) tortuosity of the active material, (e) tortuosity of the solid electrolyte and (f) diameter of the AM-specific contact area. (For interpretation of the references to color in this figure legend, the reader is referred to the Web version of this article.)

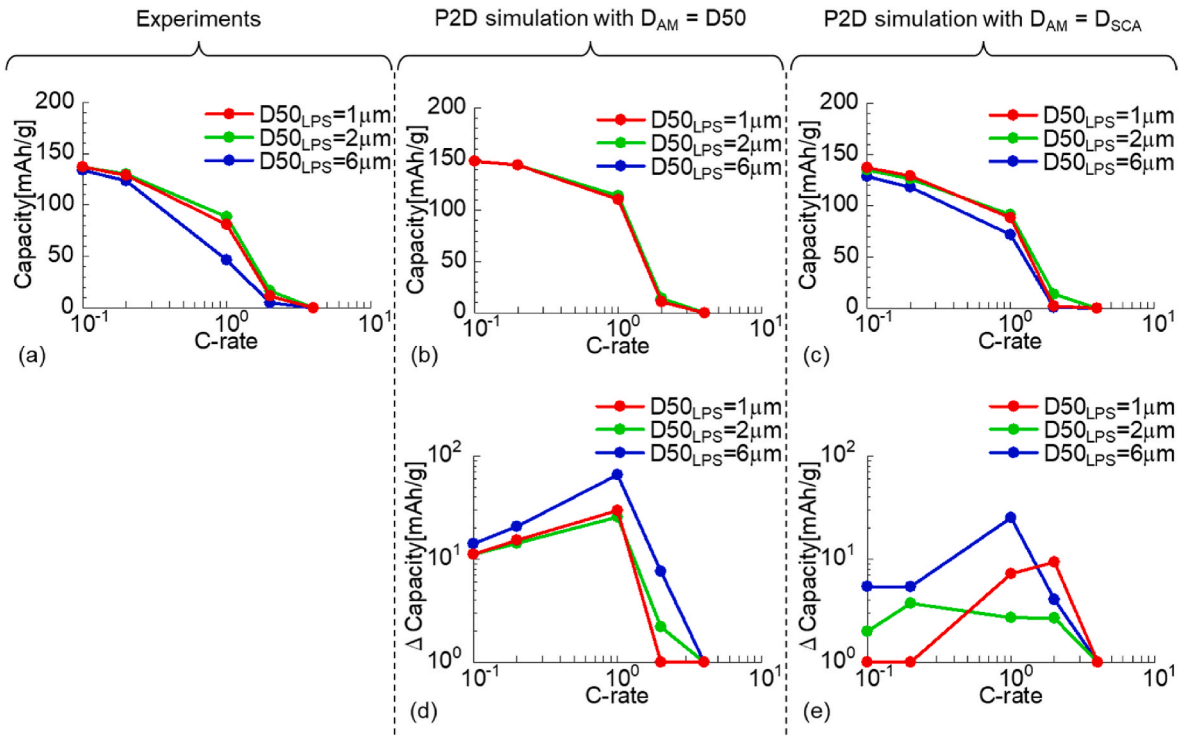

Fig. 2. (a)–(c) Discharge capacities and (d)–(e) absolute differences between experimental and simulated capacities (Δ Capacity) as functions of C-rates. These data were acquired (a) experimentally, (b) (d) using simulations involving AM median diameters, and (c) (e) using simulations incorporating D_{SCA} values.

the calculation of the contact area would also increase the simulation accuracy.

Fig. 4 summarizes the 2D Li concentration distribution in the AM particles at the end of a 1 C discharge for varying SE particle sizes as predicted by P2D simulations. Fig. 4 (a), (b) and (c) present results obtained with $D50_{AM}$ for SE particle sizes of 1, 2 and 6 μm, respectively, while Fig. 4 (d), (e) and (f) show the distributions generated with D_{SCA} for these same particle sizes. In these plots, the Li concentrations are indicated by variations in color. The distribution throughout the AM particle radius is along the vertical axis while that in the electrode thickness direction is along the horizontal axis. Therefore, in these graphs, the maximum radius value is the AM particle size and the

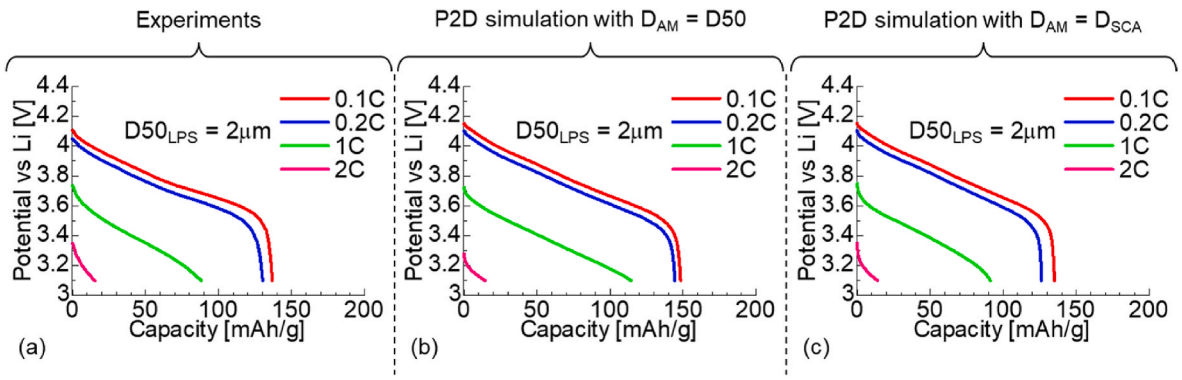

Fig. 3. Discharge curves acquired from (a) experiments, (b) simulations involving AM median diameters, and (c) simulations involving AM-specific contact area diameters for 2-μm solid electrolyte particles.

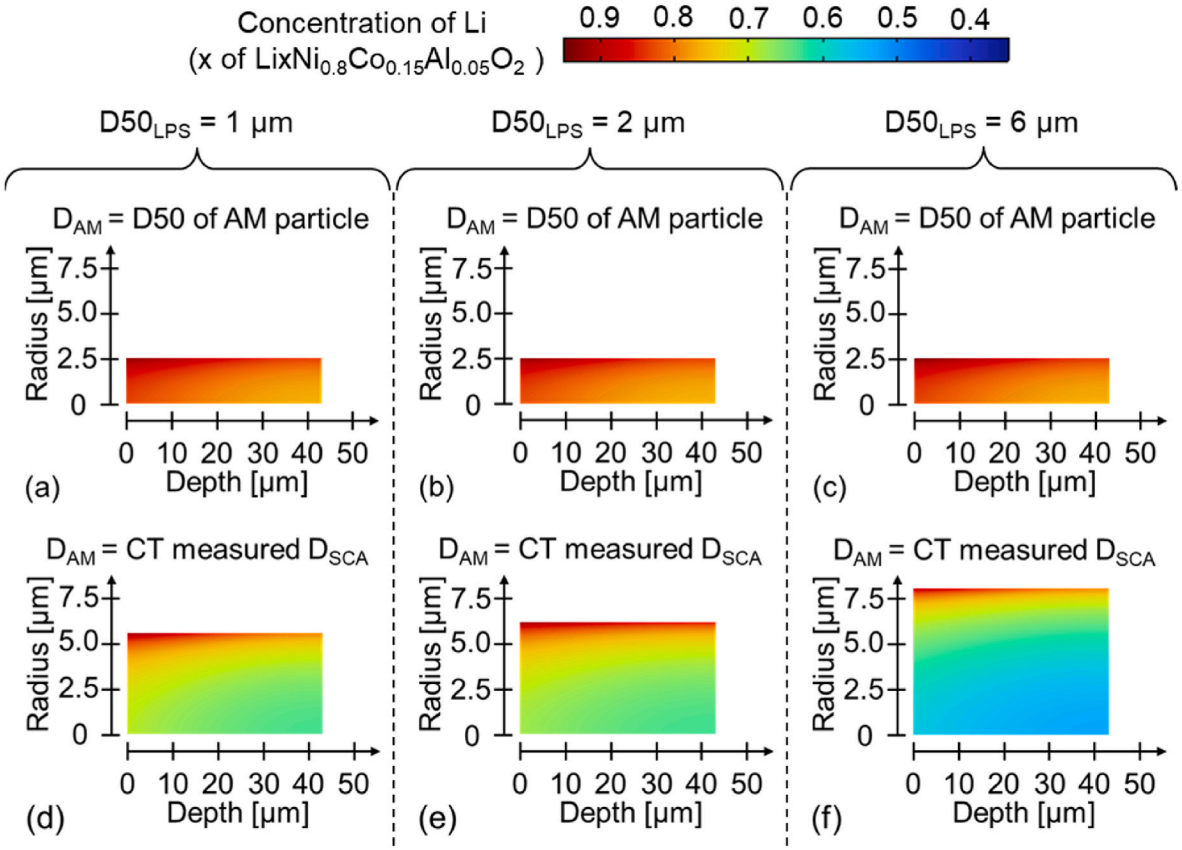

Fig. 4. Li concentration distributions at the end of discharge obtained using AM median diameters in conjunction with SE particle sizes of (a) $D50_{LPS}$ = 1 μm, (b) $D50_{LPS}$ = 2 μm and (c) $D50_{LPS}$ = 6 μm, and using D_{SCA} values with SE particle sizes of (d) $D50_{LPS}$ = 1 μm, (e) $D50_{LPS}$ = 2 μm and (f) $D50_{LPS}$ = 6 μm.

maximum depth value equals the electrode thickness. In the case of the simulations performed using $D50_{AM}$, the Li concentration distribution in the AM was not changed by varying the SE particle size and was higher than 0.8 in all regions, meaning that all AM particles in the electrode would have been almost fully discharged. This result explains the high capacity in the simulations with $D50_{AM}$ shown in Fig. 2 (b) and 3 (b). In contrast, the simulations with D_{SCA} indicated that the Li concentration at the center of the AM particle is less than 0.65, and is even lower at deeper electrode location and larger SE particle sizes. These low Li concentrations are ascribed to the larger effective particle sizes produced by aggregation and the longer diffusion length from the surface of the AM particle (that is, the SE-AM interface) to the center of the AM particle. Lower Li concentrations would, in turn, decrease the battery capacity and so the P2D simulations using D_{SCA} accurately reproduced Li diffusion in AM particle aggregates at various SE particle sizes.

4. Conclusions

A method allowing highly accurate P2D simulations of ASSLiBs using the Newman model in conjunction with D_{SCA} values has been demonstrated. Simulations incorporating the volume fraction and tortuosity values calculated from X-ray CT images together with the AM median diameter were found not to accurately reproduce experimental data. In contrast, the use of D_{SCA} values obtained from such images in place of the AM median diameter provided good agreement with the experimental results because AM particle aggregation and Li diffusion in the AM particles were properly simulated.

This study developed a high-accuracy P2D simulation and found that

decreasing SE particle size reduces AM aggregation, resulting in a shorter lithium diffusion distance and improved discharge capacity. This suggests that battery performance can be improved by reducing both active material aggregation and AM atomization.

CRediT authorship contribution statement

S. Iwamoto: Writing - Original draft, Methodology, Investigation, Resources.

M. Kodama: Writing - Review & Editing, Conceptualization, Software.

K. Yanagi: Conceptualization, Investigation, Data Curation.

Y. Haniu: Investigation.

Y. Fuji: Investigation.

N. Masuda: Investigation.

H. Higuchi: Conceptualization, Supervision.

Y. Suetsugu: Project administration, Funding acquisition.

S. Hirai: Project administration, Supervision.

Declaration of competing interest

The authors declare that they have no known competing financial interests or personal relationships that could have appeared to influence the work reported in this paper.

Data availability

Data will be made available on request.

Acknowledgements

This work was supported by Idemitsu Kosan Collaborative Research Cluster for Advanced Materials (IKCRCAM) in Tokyo Tech open innovation platform. The authors would like to thank Prof. Takeshi Kikutani, the research director of IKCRCAM, for the useful discussions and the support of this work.

References

[1] J.-M. Tarascon, M. Armand, Issues and challenges facing rechargeable lithium batteries, Nature 414 (2001) 359–367, https://doi.org/10.1038/35104644.

[2] K. Liu, Y. Liu, D. Lin, A. Pei, Y. Cui, Materials for lithium-ion battery safety, Sci. Adv. 22 (2018) 4, https://doi.org/10.1126/sciadv.aas9820, eaas9820.

[3] C. Sun, J. Liu, Y. Gong, D.P. Wilkinson, J. Zhang, Recent advances in all-solid-state rechargeable lithium batteries, Nanomater. Energy 33 (2017) 363–386, https://doi.org/10.1016/j.nanoen.2017.01.028.

[4] Z. Siroma, T. Sato, T. Takeuchi, R. Nagai, A. Ota, T. Ioroi, AC impedance analysis of ionic and electronic conductivities in electrode mixture layers for an all-solid-state lithium-ion battery, J. Power Sources 316 (2016) 215–223, https://doi.org/10.1016/j.jpowsour.2016.03.059.

[5] F. Strauss, T. Bartsch, L. de Biasi, A.Y. Kim, J. Janek, P. Hartmann, T. Brezesinski, Impact of cathode material particle size on the capacity of bulk-type all-solid-state batteries, ACS Energy Lett. 3 (2018) 992–996, https://doi.org/10.1021/acsenergylett.8b00275.

[6] M. Otoyama, Y. Akitoshi, H. Masahiro, Raman imaging for LiCoO2 composite positive electrodes in all-solid-state lithium batteries using Li_2S–P_2S_5 solid electrolytes, J. Power Sources 302 (2016) 419–425, https://doi.org/10.1016/j.jpowsour.2015.10.040.

[7] V. Ramadesigan, P.W.C. Northrop, S. De, S. Santhanagopalan, R.D. Braatz, V. R. Subramanian, Modeling and simulation of lithium-ion batteries from a systems engineering perspective, J. Electrochem. Soc. 159 (2011) R31–R45, https://doi.org/10.1149/2.018203jes.

[8] N. Legrand, S. Raël, B. Knosp, M. Hinaje, P. Desprez, F. Lapicque, Including double-layer capacitance in lithium-ion battery mathematical models, J. Power Sources 251 (2014) 370–378, https://doi.org/10.1016/j.jpowsour.2013.11.044.

[9] J. Newman, W. Tiedemann, Porous-electrode theory with battery applications, AIChE J. 21 (1975) 25–41, https://doi.org/10.1002/aic.690210103.

[10] N. Wolff, F. Roeder, U.J.E.A. Krewer, Model Based Assessment of Performance of Lithium-Ion Batteries Using Single Ion Conducting Electrolytes, vol. 284, 2018, pp. 639–646, https://doi.org/10.1016/j.electacta.2018.07.125.

[11] D.A. Bruggeman, Berechnung verschiedener physikalischer konstanten von heterogenen substanzen, Ann. Phys. Lpz. 24 (1935) 636–664, https://doi.org/10.1002/andp.19354160705.

[12] Z. Zhang, Z. Wang, L. Zhang, D. Liu, C. Yu, X. Yan, J. Xie, J. Huang, Unraveling the conversion evolution on solid-state Na–SeS 2 battery via in situ TEM, Adv. Sci. 9 (2002), 2200744, https://doi.org/10.1002/advs.202200744.

[13] T. Knorr, S. Hein, B. Prifling, M. Neumann, T. Danner, V. Schmidt, A. Latz, Simulation-Based and Data-Driven Techniques for Quantifying the Influence of the Carbon Binder Domain on Electrochemical Properties of Li-Ion Batteries, vol. 15, Multidisciplinary Digital Publishing Institute, 2022, pp. 1–19, https://doi.org/10.3390/en15217821.

[14] D. Hlushkou, A.E. Reising, N. Kaiser, S. Spannenberger, S. Schlabach, Y. Kato, B. Roling, U. Tallarek, The influence of void space on ion transport in a composite cathode for all-solid-state batteries, J. Power Sources 396 (2018) 363–370, https://doi.org/10.1016/j.jpowsour.2018.06.041.

[15] A.G. Kashkooli, S. Farhad, D.U. Lee, K. Feng, S. Litster, S.K. Babu, L. Zhu, Z. Chena, Multiscale modeling of lithium-ion battery electrodes based on nano-scale X-ray computed tomography, J. Power Sources 307 (2016) 496–509, https://doi.org/10.1016/j.jpowsour.2015.12.134.

[16] C.W. Wang, A.M. Sastry, Mesoscale modeling of a Li-ion polymer cell, J. Electrochem. Soc. 154 (11) (2007) A1035–A1047, https://doi.org/10.1149/1.2778285.

[17] A. Awarker, S. Lauer, S. Pischinger, M. Wittler, Percolation–tunneling modeling for the study of the electric conductivity in LiFePO4 based Li-ion battery cathodes, J. Power Sources 196 (2011) 405–411, https://doi.org/10.1016/j.jpowsour.2010.07.048.

[18] G.M. Goldin, A.M. Colclasure, A.H. Wiedemann, R.J. Kee, Three-dimensional particle-resolved models of Li-ion batteries to assist the evaluation of empirical parameters in one-dimensional models, Electrochim. Acta 64 (2012) 118–129, https://doi.org/10.1016/j.electacta.2011.12.119.

[19] M. Kodama, A. Ohashi, H. Adachi, T. Miyuki, A. Takeuchi, M. Yasutake, K. Uesugi, T. Kaburagi, S. Hirai, Three-dimensional structural measurement and material identification of an all-solid-state lithium-ion battery by X-Ray nanotomography and deep learning, J. Power Sources Adv. 8 (2021), 100048, https://doi.org/10.1016/j.powera.2021.100048.

[20] A. Ohashi, M. Kodama, S. Xueying, S. Hori, K. Suzuki, R. Kanno, S. Hirai, Stress Distribution in the Composite Electrodes of Sulfide All-Solid-State Lithium-Ion Batteries, vol. 470, 2020, 228437, https://doi.org/10.1016/j.jpowsour.2020.228437.

[21] A. Ohashi, M. Kodama, N. Horikawa, S. Hirai, Effect of young's modulus of active materials on ion transport through solid electrolyte in all-solid-state lithium-ion battery, J. Power Sources 483 (2021), 229212, https://doi.org/10.1016/j.jpowsour.2020.229212.

[22] M. Kodama, S. Komiyama, A. Ohashi, N. Horikawa, K. Kawamura, S. Hirai, High-pressure in situ X-ray computed tomography and numerical simulation of sulfide solid electrolyte, J. Power Sources 462 (2020), 228160, https://doi.org/10.1016/j.jpowsour.2020.228160.

[23] D.W. Dees, K.G. Gallagher, D.P. Abraham, A.N. Jansen, Electrochemical modeling the impedance of a lithium-ion positive electrode single particle, J. Electrochem. Soc. 160 (2013) A478–A486, https://doi.org/10.1149/2.055303jes.